
# Effect of the Plastic Hinge and Boundary Conditions on the Impact Behavior of Reinforced Concrete Beams

Thong M. Pham , Hong Hao

PII: S0734-743X(16)30585-1
DOI: 10.1016/j.ijimpeng.2016.12.005
Reference: IE 2789

To appear in: *International Journal of Impact Engineering*

Received date: 30 August 2016
Revised date: 5 December 2016
Accepted date: 9 December 2016

Please cite this article as: Thong M. Pham , Hong Hao , Effect of the Plastic Hinge and Boundary Conditions on the Impact Behavior of Reinforced Concrete Beams, *International Journal of Impact Engineering* (2016), doi: 10.1016/j.ijimpeng.2016.12.005

**Highlights**

- Definition of a relatively long beam in impact behavior.
- Effect of plastic hinge on the impact behavior.
- Effect of boundary condition on the impact behavior.

# Effect of the Plastic Hinge and Boundary Conditions on the Impact Behavior of Reinforced Concrete Beams

Thong M. Pham[1] and Hong Hao[2]

**Abstract**

This study numerically investigates the effect of the plastic hinge and boundary conditions on the behavior of reinforced concrete (RC) beams under slow-impact-velocity events. Numerical models are developed by using LS-Dyna and verified against experimental results. The effect of different factors including the impact velocity, projectile weight, and concrete strength on the impact behavior of RC beams is examined. The numerical results have shown that the effect of boundary condition is marginal on the impact force but significant on the displacement and damage of relatively long beams. Determining the structural stiffness of a beam in an equivalent single degree of freedom model for predicting the impact load should consider the plastic hinge formation and stationary location. And this model is not necessarily suitable for predicting the peak beam response since it is independent of the boundary conditions when the impact velocity is fast. The negative bending moment of the simply-supported beam occurs with a large magnitude which needs to be taken into account in the design. The residual displacement is more sensitive to the boundary conditions than the peak displacement. Varying concrete strength from 20 MPa to 100 MPa does not noticeably change the impact force and displacement but significantly affects the failure mode of the beam.

**Keywords**: Plastic hinge; impact loading; impact response; amplification factor; RC beam.

[1]Research Fellow, Center for Infrastructural Monitoring and Protection, School of Civil and Mechanical Engineering, Curtin University, Kent Street, Bentley, WA 6102, Australia. Email: thong.pham@curtin.edu.au

[2]John Curtin Distinguished Professor, Center for Infrastructural Monitoring and Protection, School of Civil and Mechanical Engineering, Curtin University, Kent Street, Bentley, WA 6102, Australia (corresponding author). Email: hong.hao@curtin.edu.au

## 1. Introduction

Reinforced concrete (RC) structures have been widely used for centuries but the understanding of the impact behavior of these structures against impact loads is still limited. Several design codes based on an equivalent static approach provide general principles for the design of structures under impact loads. BSI [1] provides a guide for determining an equivalent static force on structures in an impact event, for instance, ship impact or vehicle collision. AASHTO [2] provides an empirical equation to determine the equivalent static vessel impact force depending on the impact velocity and deadweight tonnage of the vessel. The dynamic analysis of the impact process is not required in the current design codes. In reality, the shear force and bending moment of RC beams under impact are significantly different from those under static loads [3-9]. Upon impact, a stress wave is generated and propagates in the structure. Depending on the impact intensity and velocity and structural parameters, the RC beam might suffer significant local damage even before the stress wave reaches the boundary. Therefore the boundary reaction force is zero during this period and the impact force is resisted primarily by the inertial force of the beam. It is difficult for an equivalent static analysis to reflect such response and damage characteristics of RC beams subjected to impact loads.

Under large impact, a plastic hinge is expected to be formed first at the impact location and propagates along the beam. The formation of plastic hinges also affects the dynamic behavior of the RC beams. Previous studies provided discussions of the plastic hinges in the impacted RC beams [5, 10]. Pham and Hao [10] investigated the formation of the plastic hinges and proposed a procedure to predict the position of the plastic hinge and stationary point, the point that beyond it the portion of the beam has not been activated yet to resist the impact force during the impacting process, in an RC beam. Pham and Hao [10] suggested that if the

stationary point has not reached the boundary at the peak impact force in the impact event, the boundary conditions have a minimal effect on the impact force, which depends on the interaction between the impactor and the beam. Such a beam is defined as a relatively long beam and it is within the scope of this study. However, the boundary conditions affect the vibration and the impact response of an RC beam during the free-vibration phase, i.e., after the action of the impactor. From the review of the previous studies, the effect of the plastic hinge and boundary conditions on the impact behavior of RC beams has not been well investigated. This study thus examines the responses of relatively long RC beams under impact loads. The impact force, mid-span displacement, shear force, and bending moment of RC beams with different boundary conditions are quantitatively evaluated.

The effects of some critical factors on the impact behavior of RC beams are discussed in this study. These include the structural stiffness, the boundary conditions, and the impact energy in slow-impact-velocity events. A 3D finite element model is developed by using the commercial software LS-DYNA [11]. The model is validated against the experimental testing results of the impact tests on RC beams reported by Pham and Hao [12]. Using the verified numerical model, intensive simulations are carried out to study the effect of the formation of plastic hinges, different boundary conditions, beam material properties, structural stiffness and impact energy on the dynamic behavior of RC beams.

## 2. Impact Behavior of RC Beams

### *2.1. Effect of structural stiffness*

The impact force and displacement of RC beams can be predicted by using the common spring-mass models of either single degree of freedom (SDOF) or two DOF [13]. A review of the existing models was presented in the study by Pham and Hao [3]. The two DOF spring-

mass model has one spring representing the local indentation of the beam ($k_1$), another spring representing the linear stiffness of the structure ($k_2$), the mass of the projectile ($G_1$) and the effective mass of the structure ($G_2$) as shown in Fig. 1. The equations of motion can be written as [13]:

$$G_1 \ddot{x}_1 + k_1(x_1 - x_2) = 0 \quad (1)$$

$$G_2 \ddot{x}_2 + k_2 x_2 + k_1(x_2 - x_1) = 0 \quad (2)$$

where $x_1$ and $x_2$ are movements of the projectile and the beam, respectively. Meanwhile, the equation of motion of the corresponding SDOF model is:

$$G\ddot{x} + k_b x + k_m x^3 = 0 \quad (3)$$

where $k_b$ is the stiffness of the structure representing the bending flexural and $k_m$ is the stiffness of the structure accounting for the membrane effect. This model requires iterative solutions which are not straightforward to use and moreover no such models have been calibrated against RC beams yet. In addition, determination of the various parameters in a real impact case is also not an easy task. For example, the stiffness of the beam deformation and indentation are not necessarily constants under large impact loads. They not only depend on the structural dimensions and material properties, but also are strongly affected by the interaction between the impactor and the beam, and the magnitude of impact loads and structural deformation. If the impact velocity is fast at which the localized beam damage is expected, the beam displacement is governed by the local rather than the global response. In such cases, the SDOF model developed based on the global structural stiffness may not yield good predictions of the structural response. The two DOF model is expected to provide better predictions as both the local and global stiffness are considered in the model (see Equations 1 and 2). Accordingly, the effect of the material properties dominating the beam stiffness is examined in this study.

### *2.2. Effect of boundary conditions*

The boundary conditions considered in this study include simply supported and fixed ends. When an RC beam is excessively struck by a projectile, a plastic hinge is formed and travels along the beam. If the stationary points do not reach the boundary before the impact force elapses, the boundary conditions do not considerably affect the impact force [10]. As expected, the boundary conditions were experimentally found to have a marginal effect on the impact force but significant effect on the displacement [14]. Han et al. [14] conducted impact tests on 12 circular concrete filled steel tubular specimens which satisfied the definition of a relatively long beam in this study. Two types of the boundary conditions were investigated, including simply-supported and fixed-end beams. The experimental results showed the boundary conditions had a marginal effect on the impact force but significantly influenced the mid-span displacement. The time histories of the tested beam showed multiple peaks of the impact force at which the first peak was exceptionally high compared to the others. Regarding the first impulse, the peak impact forces and duration of the tested beams with different boundary conditions were almost the same. The total duration of the impact force was slightly different from each other because of the influence of the boundary conditions in a later stage. The observation was based on the experimental results of concrete filled steel tubes and was not explained and verified against a wide range of the impact velocity and reinforced concrete beams. It should be noted that this phenomenon can be expected in relatively long beams. It may not be correct when the beam is short so that stress wave can reach the beam boundary quickly during the impact. However, this observation has not been verified with RC beams although it was mentioned in the previous study by Pham and Hao [10], in which the effect of the plastic hinge and boundary conditions on the impact behavior of RC beams is examined against a wide range of impact velocity varying from 1 m/s to 12 m/s.

## 3. Experimental Testing

### *3.1. Specimen design and material properties*

The experimental testing reported by Pham and Hao [12] is adopted here to validate the numerical model. The section of the tested rectangular RC beams was 150 mm in width, 250 mm in height, and 2200 mm in length. The beams had the longitudinal reinforcements consisting of 2D12 and 2D10 and the shear reinforcements of D10 at the spacing of 125 mm. The nominal tensile strength of the reinforcement was 500 MPa. The ready-mixed concrete used to cast these beams had the compressive strength of 46 MPa at 28-day age.

### *3.2. Test setup*

Drop-weight impact tests were conducted by dropping a weight from a certain height onto the midspan of the beam using the impact test apparatus. The weight was made of a solid steel cylinder, weighing 203.5 kg. Details of the projectile design can be found in the previous study [15]. The projectile was dropped from 2 m height to generate an impact velocity of 6.26 m/s. The boundary condition was carefully designed for center-point flexural impact tests of the simply supported beams. A pin and a steel roller were placed on the supports to produce an effective span of 1900 mm (see Fig. 2).

## 4. Numerical Model Development

### *4.1. FE model*

The numerical simulation is carried out by using the commercial software LS-DYNA which is based on explicit numerical methods [11]. This software has been widely used to analyze the problems associated with large deformation, structural response to impact and blast loads,

and strain rate behavior of materials. The software has been proven yielding reliable numerical predictions of structural responses to impact loads [16-21].

A numerical model is developed in LS-Dyna to simulate the experimental impact tests reported by Pham and Hao [12]. 8-nodes constant stress solid element (SOLID_164) with 1-point quadrature integration is employed to model the concrete and the steel plates while 3-nodes beam element (BEAM_161) with 2 x 2 Gauss quadrature integration is used for reinforcements. The model contains 2036 beam elements and 109418 solid elements. A perfect bond between reinforcements and surrounding concrete is assumed. The mesh convergence test is conducted by halving the mesh size. The results show that the numerical simulation converges when the mesh size is 10 mm. Further reducing the element size only has insignificant influence on the numerical results but increases the computing time and the risk of the computer memory overflow. Thus, 10 mm mesh is used in this numerical model.

Two boundary conditions including simply supported and fixed ends are investigated in this study. The simply supported condition in the experimental tests was described in the previous study [12] and shown in Fig. 2. To ensure the boundary condition in the numerical model and experimental test are identical, the actual structure of the support is simulated in the numerical model including the steel plates and rollers, which are modelled with solid elements. As previously investigated, the accurate finite element model of the boundary conditions was found to be essential for yielding reliable numerical results [22]. For the fixed-end condition, the end nodes are constrained in all degrees of freedom. The solid steel projectile is modeled with the actual shape by using solid elements. The projectile had a cylindrical shape, machined from a 260-mm-diameter steel cylinder, with a half-spherical head. The top head of the projectile was a flat circular surface with a radius of 50 mm. Details of the numerical model, projectile, and the supports are presented in Fig. 3. The penalty contact algorithm

*Contact_automatic_Surface_to_Surface is used to simulate the contact between the steel plates, steel rollers, and the concrete beam at the supports.

### *4.2. Material model*

LS_Dyna provides a number of constitutive models (e.g. MAT 16, 25, 72, 84/85, and 159) to represent the concrete behavior under impact and blast loads. Some of these available models have been adopted to simulate concrete against impact loads and their verification has been confirmed by previous studies [17, 23-25]. In this study, the material model *Mat_Concrete_Damage_Rel3 (MAT_72_REL3) is used to simulate the concrete behavior. This material model takes into account the strain-rate effect, plasticity and damage softening after failure. Previous studies have shown that this material model yielded reliable numerical predictions of concrete structures against impact and blast loads [25-28]. The material model is based on the concrete compressive strength of 46 MPa.

Meanwhile, the steel reinforcements, load adaptor and plates are modeled by using the material model *Mat_Piecewise_Linear_Plasticity (MAT_24). The mass density, elastic modulus, and yield stress of the reinforcements and steel plates are 7800 kg/m$^3$, 200 GPa, and 500 MPa, respectively. The isotropic and kinematic hardening plasticity is considered in this material model. It allows users to define parameters for the required stress-strain curve and the strain rate curve. In addition, the card *Mat_Add_Erosion is used to eliminate concrete elements which are no longer contributing to resisting the impact load. This study uses the maximum principal strain at failure as a criterion to delete the failed concrete elements while no erosion criteria is applied for other materials. The value of 0.15 is used after trials to yield fairly good agreement with the experimental results. It is noted that the erosion criterion is used to simulate the concrete material damage. The numerical simulation is also carried out without applying the erosion criterion to examine its effect on the results. The differences

between models with and without erosion criterion are trivial. This is because the concrete damages of the considered cases do not cause simulation overflow although significant concrete cracks appear. The simulation results obtained with application of erosion criterion are adopted here because they clearly show the concrete cracks.

### *4.3. Strain rate effect*

Under impact and blast loads, the inertia and strain-rate effects are dominant factors to the structural response, which is different from the quasi-static scenario. In such cases, both concrete and steel may respond at very high strain rates in the order of 10 - 1000 $s^{-1}$. The strength of these materials corresponding to high strain rates can be significantly higher than the strengths under static loads [29]. The strength increase of the steel reinforcement was observed up to more than 50% in the experiment as reviewed by Malvar [30]. The corresponding increase of the compressive and tensile strength of concrete under high strain rate could be up to 100% and 600%, respectively [31]. Therefore, the strain rate effect of concrete and steel reinforcement needs to be taken into account in the simulation to ensure reliable numerical results.

The strength increment is defined by the dynamic increase factor (DIF) at a given strain rate. Hao et al. [32] conducted a review about the concrete dynamic material properties. It was concluded that DIF was a material property although those obtained directly from high-speed impact tests contain contributions from other sources such as inertia and friction confinements. This statement agrees with results from previous studies [33-35]. Many empirical models have been proposed in the literature to quantify the strain rate effect of concrete and steel. The use of DIF to model the strain rate effect of concrete and steel materials associated with high strain rate was proven to yield reliable predictions [27-29]. Hao and Hao [29] have proposed a new DIF relation for concrete material, in which the

contribution to strength increment from lateral inertia confinement associated with the high-speed impact tests has been removed. The accuracy of the proposed model had been experimentally verified by the split Hopkinson pressure bar tests [35]. The DIF relations for concrete material used in this study are presented in the following expressions:

$$CDIF = \frac{f_{cd}}{f_{cs}} = 0.0419(\log \dot{\varepsilon}_d) + 1.2165 \quad for \quad \dot{\varepsilon}_d \le 30/s \tag{4}$$

$$CDIF = \frac{f_{cd}}{f_{cs}} = 0.8988(\log \dot{\varepsilon}_d)^2 - 2.8255(\log \dot{\varepsilon}_d) + 3.4907 \quad for \quad \dot{\varepsilon}_d > 30/s \tag{5}$$

$$TDIF = \frac{f_{td}}{f_{ts}} = 0.26(\log \dot{\varepsilon}_d) + 2.06 \quad for \quad \dot{\varepsilon}_d \le 1/s \tag{6}$$

$$TDIF = \frac{f_{td}}{f_{ts}} = 2(\log \dot{\varepsilon}_d) + 2.06 \quad for \quad \dot{\varepsilon}_d \le 1/s \tag{7}$$

$$TDIF = \frac{f_{td}}{f_{ts}} = 1.4431(\log \dot{\varepsilon}_d) + 2.2276 \quad for \quad \dot{\varepsilon}_d \le 1/s \tag{8}$$

where CDIF and TDIF are the DIF for concrete in compression and tension, respectively; $f_{cd}$ and $f_{cs}$ are the compressive strength of concrete at high strain rate and quasi-static loads, respectively; $f_{td}$ and $f_{ts}$ are the tensile strength of concrete at high strain rate and quasi-static loads, respectively; and $\dot{\varepsilon}_d$ is the strain rate.

### *4.4. Model verification*

The numerical simulation results are verified against the experimental results as shown in Figs. 4-5. Fig. 4 shows the plastic strain along the beam, in which high plastic strain occurs at the mid-span. Concrete crushing is observed at the impact point in both the numerical and experimental results. As previously observed in the experiment, the combined failure mode of shear and flexural damage is observed in the numerical model. The two major shear cracks can also be seen in both the experiment and simulation. Fig. 5 shows the time histories of the mid-span displacement and the impact force of the tested beam. The numerical results for the

maximum and residual displacement of the beam agree well with those from the experimental testing. The maximum displacement in the two cases occurs at about 25 ms and the free vibration phase decays at approximately 100 ms. In addition, the impact force in the simulation also agrees well with those from the experiment as shown in Fig. 5. There are two peaks observed in both the experiment and the simulation, at which the second peak occurs at 10 ms after the first peak. Details of the dynamic response of the beam was presented in the study by Pham and Hao [12]. In general, the dynamic response of the beam observed in the experimental testing is well simulated in the numerical model and the verification has shown that the numerical model yields reliable predictions of the RC beam response to impact loads.

## 5. Numerical Investigations on Boundary Condition Effect

As previously mentioned, if a beam is relatively long, the boundary conditions have a minimal effect on the impact force but significant influence on the mid-span displacement [10]. The present study further investigates the boundary condition effect on the response of the relatively long RC beams through numerical simulations. It should be noted that here the term 'relatively long beam' refers to the beam that stationary points do not reach the boundary when the impact force reaches the peak. It does not refer to any beam with a specific length as this condition depends not only on the length of the beam but also on the impact velocity, and interaction between beam and impactor.

### *5.1. Impact force and displacement time histories*

The numerical simulations are carried out on the tested beam described above, i.e., the 150x250 mm rectangular beam impacted by a 203.5 kg projectile with the impact velocity of 6.26 m/s. Fig. 6 shows the impact force time histories of the simply-supported and fixed-end beams. The figure clearly shows that the boundary conditions do not affect the peak impact

force but the impact duration. The first and the second peak of the impact forces of the two beams are almost identical. This is because the beam simulated in this study is relatively long and the stationary point has not reached the supports at the instant of the maximum impact force. Based on discussions from the study of the same beam model by Pham and Hao [10], the stationary points arrived at the supports only when the impact force almost elapses. As presented in the latter study, the impact force reached the peak value at 0.26 ms and the stationary point traveled a distance of 0.7 m from the midspan at the same instant. It is worth noting that the projectile is actually positioned at 10 mm above the load adaptor with a given velocity in the simulation. This treatment is to avoid possibly initial penetration of the concrete beams when directly placing the projectile in contact with the beam. As a result, the projectile needs 1.6 ms to reach the actual impact surface. The support was 0.95 m away from the midspan so that the stationary point had not reached the support at the instant of the maximum force. As a result, the maximum impact force of the RC beams with different boundary conditions (simply supported and fixed ends) is expected to be similar. The impact force duration, which depends on the interaction between the impactor and beam, however, is different. After the action of impact force ends, the RC beam still vibrates freely for a period much longer than the impact force duration. During the free vibration phase, the boundary condition obviously affects the beam response so that the displacements of the simply supported beam and the fixed-end beam are different. As expected, the mid-span displacement time histories of the two beams show a significant difference (see Fig. 7). The maximum displacements of the simply-supported beam and the fixed-end beam are 48 mm and 9.9 mm, respectively. The corresponding values of the residual displacement are respectively 42 mm and 4.7 mm. In addition, the simply-supported beam comes to rest at about 100 ms while the fixed-end beam reaches the stationary stage at about 50 ms because higher vibration frequency of the fixed-end beam than that of the simply-supported beam

associates with a higher damping. The residual mid-span displacement of the simply-supported beam is about 9 times larger than that of the fixed-end beam.

As demonstrated above, when the two beams are impacted with the velocity of 6.26 m/s by a projectile of 203.5 kg falling freely from 2 meters, the impact force and displacement of the both beams are similar as presented in Fig. 6 during the action of the impact, indicating the boundary conditions have almost no influence on the impactor-beam interaction. This observation, however, has not been verified with other impact scenarios. As discussed above, this is caused primarily because the stress wave does not reach the boundary during the impacting duration. Therefore the observation is believed highly dependent on the beam dimension and impact velocity. To investigate the influences of beam boundary conditions on the impactor-beam interaction corresponding to the different impact velocities, the above simulations are carried out again with different impact velocities in the range between 1 m/s and 12 m/s (the projectile weight kept unchanged). The impact force time histories of the two beams with the impact velocities of 1 m/s and 12 m/s are presented in Figs. 8-9, respectively. As shown, under the slow impact velocity of 1 m/s, the impact force exhibits multiple peaks and the first impulses are identical on the two beams. The duration of the first impulse of about 1 ms is similar to the impact under the velocity of 6.26 m/s. The first peak impact force of the two beams reaches the value of 160 kN at the same time as shown in Fig. 8. Similar to the case of 1 m/s, the impact force time histories of the two beams are almost identical when the impact velocity is 12 m/s (see Fig. 9). Therefore, the first impulse of the impact force is not affected by the boundary conditions during this impact velocity range for the beam under consideration.

The damage of the RC beams corresponding to the impact velocity of 6.26 m/s, resulting from dropping the projectile from 2 m height, is presented in Fig. 10. The plastic strain, indicating

the plastic deformation of the beams, of the two beams is almost identical up to about 2.4 ms when the farthest plasticized element reaches the supports. It is noted that the projectile impacts the beams at about 1.6 ms and the impact force is decaying at about 2.4 ms as shown in Fig. 6. Therefore, the statement that the boundary conditions do not affect the maximum impact force of these beams is again confirmed. The difference of the impact forces of the two beams only appears when the farthest plasticized element reaches the boundary at about 2.4 ms as shown in Fig. 6. After the force phase, the boundary conditions affect the response of the beams during the free vibration phase. In the free vibration phase, the simply-supported beam has two major shear cracks which are not observed in the fixed-end beams as shown in Fig. 10. The fixed-end beam shows damage on the top surface of the beam at the fixed ends where the negative moments are expected to be prominent. In addition, the positive moment at the fixed ends, which is resulted from the free vibration and does not exist in the static case, causes some plastic deformation.

In general, the impact response of RC beams under impact loads includes two phases that are the force phase and the free vibration phase. In the case of relatively long beams, the boundary conditions have no effect on the maximum impact force while it may affect the impact duration. This phenomenon indicates that the behavior of the impacted beam in the force phase is almost independent of the boundary conditions when the impact velocity is fast enough and/or the beam span is long enough, i.e., the impact velocity more than 1 m/s and beam span longer than 1.9 m in this study. On the other hand, the mid-span displacement is significantly influenced by the boundary conditions because the largest displacement response occurs in the free vibration phase when the impact force on the beam is sufficiently fast. The above observations indicate that determining the equivalent structural stiffness of an RC beam in an SDOF spring-mass model for predicting the impact force should consider the location of the plastic hinge formation because the entire beam is not necessarily activated during the

impact, but this SDOF model might not be suitable for predicting the beam response because it is likely governed by free vibrations, which is significantly influenced by boundary conditions.

### *5.2. Bending moment and shear force*

The bending moment and shear force at a particular section of the beam are evaluated by using the keyword Database_Cross_Section_Set in LS-Dyna. A cross section is defined by an element set and the forces from the elements belonging to the element set are summed up to calculate the section forces [11]. Figs. 11-14 show the time histories of the bending moment and shear force of the beams. Two critical sections are considered in this analysis: the section at 70 mm away from the mid-span (Section B-B) coinciding with the edge of the steel plate used as load adaptor in the test, shown in Fig. 2, and the section close to the support where the negative moment occurs (Section A-A). Under the impact load, there are two critical moments which are the positive moment at the mid-span and the negative moment near the supports. The time histories of the bending moment of the simply-supported beam are presented in Fig. 11. The maximum moment at the mid-span is about 35 kNm as compared to the corresponding value of 25.6 kNm under the static load as reported in the previous study [12]. The negative moment reaches the peak of -26.8 kNm at about 0.4 ms after the positive moment. It should be noted that the negative moment is also generated at the supports of the simply-supported beam. This is because the simple support condition was simulated by placing a steel plate and a roller on the both sides of the beam as shown in Figs. 2 and 3. The steel plate provides certain constraint at the support for the beam to rotate freely. As shown the first peak of positive moment lasts for approximately 1.1 ms while the corresponding duration of the negative moment is about 0.4 ms. Fig. 12 shows the bending moment time histories of the fixed-end beam. The moment of the fixed-end beam starts at the same time as

those in the simply-supported beam but it lasts longer. The duration of the first impulse of both the positive and negative moments is about 5.5 ms. It is noted that the duration of the moment impulse in the simply-supported beams is approximately 1 ms. The time lag between the positive and negative moments is also approximately 0.4 ms. The maximum values of the positive and negative moments are 49.6 kNm and -64.3 kNm, respectively. In general, the positive and negative moments always exist in both the beams regardless the boundary conditions. The bending moment in the fixed-end beam has larger magnitude and longer duration than those of the simply-supported beam.

The shear forces time histories of the two beams have a similar trend to that of the bending moment as presented in Figs. 13-14. Unlike the static case, the shear forces at the mid-span and the support of the beam have significantly different values and they may act on the two opposite directions at an instant during the impact. This phenomenon was experimentally observed and qualitatively reported in the previous studies [5, 12, 36, 37]. The positive shear forces at the mid-span of the two beams reach the maximum value at about 360 kN. The maximum positive shear forces are observed to be much greater than the maximum negative shear forces. The positive shear forces of the two cases almost stay in the positive side of the graphs while the negative shear forces move into the positive side at the later stage. The maximum negative shear forces of the simply-supported and fixed-end beams are approximately -110 kN and -250 kN, respectively. The positive and negative shear forces always appear in the impacted beams regardless their boundary conditions. Because the direction of the negative shear forces changes, the direction of the inclined shear reinforcement should be carefully considered in the design. In addition, the envelopes of the bending moment and shear force of simply-supported and fixed-end beams are presented in Figs. 15-16, respectively. The envelopes are produced by plotting the bending moment and shear force diagrams along the beam at 5000 time steps. As shown under impact loading, the

bending moment and shear force distribution in the beam changes significantly with time owing to wave propagation and vibration.

### *5.3. Dynamic amplification factor*

Under dynamic loads, the response of structures is generally greater than that under static loads. This increase is quantified by the dynamic amplification factor (DAF) which is defined as the ratio of the structure response under dynamic loads and static loads. There are several definitions for the DAF but the definition of the DAF adopted in this study can be expressed as follows [38, 39].

$$DAF = \frac{M_{ud}}{M_{us}} \tag{9}$$

where $M_{ud}$ and $M_{us}$ are the moment capacity of a structure under impact loads and static loads, respectively. The moment capacity under static loads is obtained from the experimental tests while the corresponding number under impact loads is derived from the numerical simulation. The moment capacity of the beam under static load is 25.6 kNm as reported in the previous study [12]. The DAF for the simply-supported beam is 1.37. It is noted that the DAF is estimated from the positive bending moment at the mid-span. In relatively long beams, the boundary conditions do not affect the maximum impact force but the bending moment and the DAF.

## 6. Effect of Different Factors on Simply-supported Beams

Based on the above numerical model of RC beams, intensive numerical simulations are also conducted to examine the influences of the impact velocity, the projectile weight, and the concrete strength on the impact behavior of the simply-supported beams as presented in Table 1.

### *6.1. Impact energy*

The values of the impact velocity and the projectile weight are changed so that their combination generates the same impact energy as the projectile of 203.5 kg dropping from 2 m height. Details of the projectile weight and the impact velocity are presented in Table 1. The damage of the simply-supported beams is presented in Fig. 17 while the mid-span displacement is shown in Fig. 18. The beam impacted by a heavier and slower projectile (300-500 kg) fails with vertical cracks in a large region at the mid-span. The damage of the beam impacted by a projectile of 300-500 kg exhibits a similar plastic strain contour. On the other hand, the beam impacted by the projectile of 50 kg with the impact velocity of 12.89 m/s shows two major shear cracks. Concrete at the negative moment region on the top surface near the supports shows large plastic strain, indicating the negative moments are significantly higher as compared to the other cases with lower impact velocities. The failure of the beam impacted with the impact velocity of 12.89 m/s is different from the others. The scabbing of the concrete cover at the middle soffit of the beam (at 1.72 ms) is observed before shear cracks appear (at 5.16 ms) as shown in Fig. 17. This failure was reported as the impact velocity increased in the tests [40, 41]. Even though these beams are impacted by the same impact energy, the faster impact velocity causes more localized damage and less global response as expected. As shown in Fig. 18, the slower impact velocity beams exhibit higher maximum and residual displacements than others. With the same impact energy, the beam impacted with faster impact velocity shows higher maximum impact force as shown in Fig. 19. The difference becomes more significant when the projectile weight is 50 kg with an impact velocity of 12.9 m/s. This change in the impact force is resulted from the projectile-beam interaction since the failure of the beam changed at the impact velocity of 12.9 m/s. Very high level of localized damage associated with scabbing of concrete is found with the impact velocity of 12.89 m/s while the global damage is observed in other impact velocities

(see Fig. 20). To evaluate the load carrying capacity of the beams under impact loads, the DAF is presented in Table 1.

### *6.2. Concrete strength*

To investigate the effect of the concrete strength on the impact behavior of the RC beam, the concrete strength of the beams is changed between 20 and 100 MPa, resulting in an increase by 30% in the concrete modulus and thus the beam stiffness. The projectile weight is 203.5 kg and the impact velocity is 6.26 m/s. The impact force increases with the concrete strength but the change is marginal (less than 5%) as shown in Fig. 21. The concrete strength also does not considerably affect the displacement since the variation is less than 5% except the beam with the concrete strength of 20 MPa. This beam shows a severe damage at which the beam is broken into portions. It is noted that the maximum displacement occurs in the free-vibration phase so that the global stiffness governs the displacement. Since the maximum difference in the beam stiffness is about 30%, the displacement is expected to have a variation of approximately 30%, which is different from the observed 5% variation. This phenomenon can be explained according to different amounts of the energy absorption in these beams. The impulse of the impact force of these beams is almost identical as shown in Fig. 21. It is assumed that the same amount of energy is transferred from the projectile to the beams. In addition, Fig. 22 shows different plastic strain contours, displaying more plastic concrete elements in the beams with lower concrete strength. As a result, more energy is dissipated in the lower-strength concrete beams due to plastic deformations. The concrete strength has an obvious influence on the failure mode as shown in Fig. 22. When the concrete strength is less than 46 MPa, the RC beams fail with vertical and inclined cracks, indicating the combined flexural-shear failure. The RC beams with the concrete strength from 60 to 100 MPa exhibit vertical cracks only, i.e., the flexural failure.

## 7. Effect of Different Factors on Fixed-end Beams

The effect of the impact velocity, the projectile weight, and the concrete strength on the impact behavior of the fixed-ended beams is numerically investigated and also presented in Table 1.

### *7.1. Impact energy*

The values of the impact velocity and the projectile weight are varied to maintain the impact energy unchanged in the simulations. Details of the projectile weight and the impact velocity are presented in Table 1. The damage and mid-span displacement of the fixed-end beams are respectively presented in Figs. 17 and 23. The beams impacted by a heavier and slower projectile (300-500 kg) exhibit minor cracks at the mid-span and the fixed ends. On the other hand, scabbing of the concrete at the soffit is observed in the beam impacted by the projectile of 50 kg with the impact velocity of 12.89 m/s. As shown in Fig. 17, the boundary condition significantly affects the damage of the beams since the corresponding beams show different plastic strain contours. The influence of the projectile weight and the impact velocity on the displacement of the fixed-end beams is less prominent than that of the simply-supported beams (see Fig. 23). There is a minor change in the displacement as the projectile weight and the impact velocity vary. The maximum mid-span displacement of these beams is between 8.2 and 10.7 mm while the corresponding residual displacement is between 1.3 and 3.6 mm.

### *7.2. Concrete strength*

The influence of the concrete strength on the impact behavior of the fixed-end beams is examined through a number of simulations. The projectile weight is 203.5 kg and the impact velocity is 6.26 m/s. Similar to the simply supported beams, the impact force in the fixed-end beams increases with the concrete strength but the change is insignificant at the level of less

than 5%. The mid-span displacement is not noticeably influenced by the concrete strength since the variation is less than 5% except the beam with the concrete strength of 20 MPa, which exhibits a severe damage.

## 8. Conclusions

This study examines the effect of plastic hinge and boundary condition on the impact behavior of relatively long RC beams, i.e., the beam with stationary points not reaching the boundary when the impact force reaches the peak. The findings in this study can be summarized as follows:

1. The effect of plastic hinge and boundary condition is marginal on the impact force but significant on the displacement of relatively long beams. This conclusion is valid for the impact velocity ranging from 1 - 12 m/s considered in the present study.

2. The maximum impact force and its duration are not influenced by the boundary conditions of relatively long beams.

3. The negative bending moment of the simply-supported beam occurs with large magnitude which needs to be taken into account.

4. The residual displacement is more sensitive to the boundary conditions than the peak displacement.

5. The scabbing of concrete was observed in the case of RC beams subjected to the impact velocity of 12.89 m/s.

6. Varying concrete strength from 20 MPa to 100 MPa does not noticeably change the impact force and displacement but it significantly affects failure mode of the beams.

Based on the results obtained in this study, it can be concluded that determining the structural stiffness of a beam in an SDOF model for predicting the impact load should consider the plastic hinge formation and stationary location. And this SDOF model is not necessarily suitable for predicting the peak beam response since it is independent of the boundary conditions when the impact velocity is fast.

**Acknowledgement**

The authors acknowledge the financial support from Australian Research Council (ARC) and Curtin University.

**References**

[1] BSI U, National annex to eurocode 1: Actions on structures–part 2: Traffic loads on bridges, NA to BS EN 1991-2: 2003, British Standards Institution 2008.
[2] AASHTO L, Bridge design specifications, in, American Association of State Highway and Transportation Officials, Washington, DC, 2012.
[3] Pham TM and Hao H, Prediction of the Impact Force on RC Beams from a Drop Weight, Adv Struct Eng 2016;19 (11):1710-1722.
[4] Pham TM and Hao H, Review of Concrete Structures Strengthened with FRP against Impact Loads, Struct 2016;7:59-70.
[5] Cotsovos DM, A simplified approach for assessing the load-carrying capacity of reinforced concrete beams under concentrated load applied at high rates, Int J Impact Eng 2010;37 (8):907-917.
[6] Kishi N and Mikami H, Empirical formulas for designing reinforced concrete beams under impact loading, ACI Struct J 2012;109 (4):509-519.
[7] Qasrawi Y, Heffernan PJ, and Fam A, Dynamic behaviour of concrete filled FRP tubes subjected to impact loading, Eng Struct 2015;100:212-225.
[8] Adhikary SD, Li B, and Fujikake K, Dynamic behavior of reinforced concrete beams under varying rates of concentrated loading, Int J Impact Eng 2012;47 (0):24-38.
[9] Goldston M, Remennikov A, and Sheikh MN, Experimental investigation of the behaviour of concrete beams reinforced with GFRP bars under static and impact loading, Eng Struct 2016;113:220-232.
[10] Pham TM and Hao H, Plastic Hinges and Inertia Forces in RC Beams under Impact Loads, Int J Impact Eng 2016;(Revision Submitted).
[11] LS-Dyna, keyword user's manual V971, 2Livermore Technology Software Corporation, Livermore, CA 2012:2994.
[12] Pham TM and Hao H, Behavior of Fiber Reinforced Polymer Strengthened Reinforced Concrete Beams under Static and Impact Loads, Int J Prot Struct 2016;DOI: 10.1177/2041419616658730.

[13] Abrate S, Modeling of impacts on composite structures, Compos Struct 2001;51 (2):129-138.
[14] Han L-H, Hou C-C, Zhao X-L, and Rasmussen KJR, Behaviour of high-strength concrete filled steel tubes under transverse impact loading, J Constr Steel Res 2014;92 (0):25-39.
[15] Pham TM and Hao H, Axial Impact Resistance of FRP-Confined Concrete, J Compos Constr 2016;10.1061/(ASCE)CC.1943-5614.0000744.
[16] Kishi N, Khasraghy SG, and Kon-No H, Numerical simulation of reinforced concrete beams under consecutive impact loading, ACI Struct J 2011;108 (4).
[17] Jiang H, Wang X, and He S, Numerical simulation of impact tests on reinforced concrete beams, Mater Design 2012;39:111-120.
[18] Dogan F, Hadavinia H, Donchev T, and Bhonge PS, Delamination of impacted composite structures by cohesive zone interface elements and tiebreak contact, Central European Journal of Engineering 2012;2 (4):612-626.
[19] Jiang H and Chorzepa MG, An effective numerical simulation methodology to predict the impact response of pre-stressed concrete members, Eng Fail Anal 2015;55:63-78.
[20] Heimbs S, Heller S, Middendorf P, Hähnel F, and Weiße J, Low velocity impact on CFRP plates with compressive preload: Test and modelling, Int J Impact Eng 2009;36 (10):1182-1193.
[21] Thilakarathna HMI, Thambiratnam D, Dhanasekar M, and Perera N, Numerical simulation of axially loaded concrete columns under transverse impact and vulnerability assessment, Int J Impact Eng 2010;37 (11):1100-1112.
[22] Villavicencio R and Guedes Soares C, Numerical modelling of the boundary conditions on beams stuck transversely by a mass, Int J Impact Eng 2011;38 (5):384-396.
[23] Jiang H and Zhao J, Calibration of the continuous surface cap model for concrete, Finite Elem Anal Des 2015;97:1-19.
[24] Tu Z and Lu Y, Evaluation of typical concrete material models used in hydrocodes for high dynamic response simulations, Int J Impact Eng 2009;36 (1):132-146.
[25] Yonten K, Manzari MT, Marzougui D, and Eskandarian A, An assessment of constitutive models of concrete in the crashworthiness simulation of roadside safety structures, Int J Crashworthiness 2005;10 (1):5-19.
[26] Malvar LJ, Crawford JE, Wesevich JW, and Simons D, A plasticity concrete material model for DYNA3D, Int J Impact Eng 1997;19 (9):847-873.
[27] Chen W, Hao H, and Chen S, Numerical analysis of prestressed reinforced concrete beam subjected to blast loading, Mater Design 2015;65:662-674.
[28] Shi Y, Hao H, and Li Z-X, Numerical derivation of pressure–impulse diagrams for prediction of RC column damage to blast loads, Int J Impact Eng 2008;35 (11):1213-1227.
[29] Hao Y and Hao H, Influence of the concrete DIF model on the numerical predictions of RC wall responses to blast loadings, Eng Struct 2014;73:24-38.
[30] Malvar LJ, Review of static and dynamic properties of steel reinforcing bars, ACI Mater J 1998;95 (5).
[31] Malvar LJ and Ross CA, Review of strain rate effects for concrete in tension, ACI Mater J 1998;95 (6).
[32] Hao H, Hao Y, Li J, and Chen W, Review of the current practices in blast-resistant analysis and design of concrete structures, Adv Struct Eng 2016:1369433216656430.
[33] Lu YB and Li QM, About the dynamic uniaxial tensile strength of concrete-like materials, Int J Impact Eng 2011;38 (4):171-180.
[34] Hao Y and Hao H, Numerical evaluation of the influence of aggregates on concrete compressive strength at high strain rate, Int J Prot Struct 2011;2 (2):177-206.

[35] Hao Y, Hao H, Jiang GP, and Zhou Y, Experimental confirmation of some factors influencing dynamic concrete compressive strengths in high-speed impact tests, Cement and Concrete Res 2013;52:63-70.
[36] Saatci S and Vecchio FJ, Effects of shear mechanisms on impact behavior of reinforced concrete beams, ACI Struct J 2009;106 (1):78-86.
[37] Pham TM and Hao H, Impact Behavior of FRP-Strengthened RC Beams without Stirrups, J Compos Constr 2016;20 (4):04016011.
[38] Paultre P, Chaallal O, and Proulx J, Bridge dynamics and dynamic amplification factors-a review of analytical and experimental findings, Can J Civ Eng 1992;19 (2):260-278.
[39] Kim S and Nowak AS, Load distribution and impact factors for I-girder bridges, J Bridge Eng 1997;2 (3):97-104.
[40] Kennedy RP, A review of procedures for the analysis and design of concrete structures to resist missile impact effects, Nuclear Engineering and Design 1976;37 (2):183-203.
[41] Yu R, van Beers L, Spiesz P, and Brouwers HJH, Impact resistance of a sustainable Ultra-High Performance Fibre Reinforced Concrete (UHPFRC) under pendulum impact loadings, Constr Build Mater 2016;107:203-215.

**List of Figures**

Figure 23. Mid-span displacement time histories of fixed-end beams with varied impact velocity and projectile weight

**List of Tables**

Table 1. Parametric study

| Simulation | Projectile weight (kg) | Impact velocity (m/s) | Concrete strength (MPa) | Boundary conditions | Max displacement (mm) | Residual displacement (mm) | DAF |
|---|---|---|---|---|---|---|---|
| S_1 m/s | 203.5 | 1 | 46 | Simply supported | 2.2 | 0.7 | - |
| S_4 m/s | | 4 | | | 22.6 | 15.8 | - |
| S_6.26 m/s | | 6.26 | | | 47.0 | 42.1 | 1.37 |
| S_9 m/s | | 9 | | | - | - | - |
| S_12 m/s | | 12 | | | - | - | - |
| S_20 MPa | 203.5 | 6.26 | 20 | Simply supported | 80.2 | 70.5 | - |
| S_60 MPa | | | 60 | | 49.1 | 44.4 | - |
| S_80 MPa | | | 80 | | 47.6 | 41.9 | - |
| S_100 MPa | | | 100 | | 47.1 | 42.1 | - |
| S_50 kg | 50 | 12.89 | 46 | Simply supported | 32.3 | 23.7 | 1.81 |
| S_100 kg | 100 | 9.11 | | | 38.0 | 3.0 | 1.69 |
| S_300 kg | 300 | 5.26 | | | 63.4 | 52.9 | 1.47 |
| S_400kg | 400 | 4.56 | | | 59.9 | 51.3 | 1.46 |
| S_500 kg | 500 | 4.08 | | | 57.1 | 50.9 | 1.44 |
| F_1 m/s | 203.5 | 1 | 46 | Fixed end | 1.0 | 0.2 | - |
| F_4 m/s | | 4 | | | 5.3 | 1.4 | - |
| F_6.26 m/s | | 6.26 | | | 9.1 | 3.3 | - |
| F_9 m/s | | 9 | | | 23.9 | 18.6 | - |
| F_12 m/s | | 12 | | | 36.8 | 28.5 | - |
| F_20 MPa | 203.5 | 6.26 | 20 | Fixed end | 28.6 | 17.1 | - |
| F_60 MPa | | | 60 | | 8.6 | 1.9 | - |
| F_80 MPa | | | 80 | | 7.3 | 0.8 | - |
| F_100 MPa | | | 100 | | 7.1 | 0.8 | - |
| F_50 kg | 50 | 12.89 | 46 | Fixed end | 8.2 | 1.3 | - |
| F_100 kg | 100 | 9.11 | | | 8.2 | 2.1 | - |
| F_300 kg | 300 | 5.26 | | | 10.1 | 3.2 | - |
| F_400kg | 400 | 4.56 | | | 10.3 | 3.1 | - |
| F_500 kg | 500 | 4.08 | | | 10.7 | 3.6 | - |

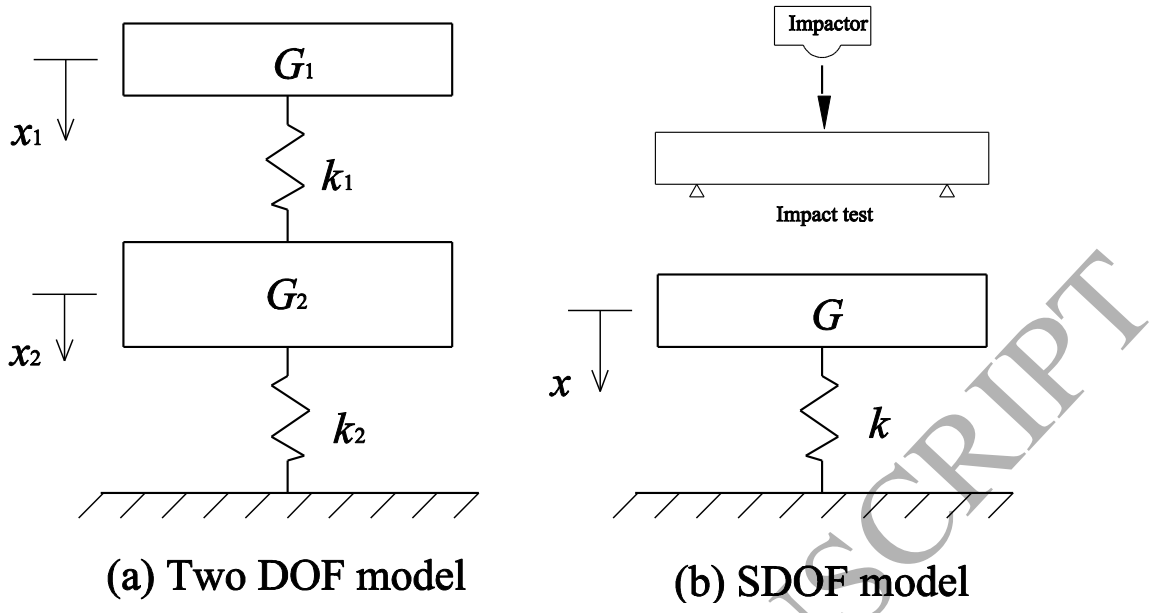


Fig 1

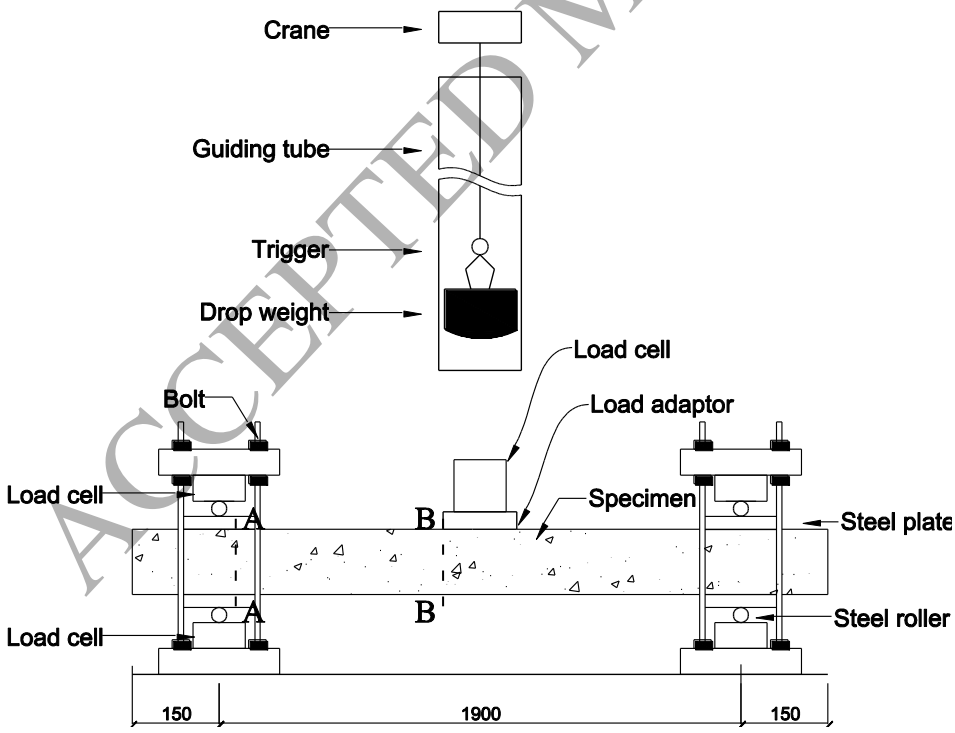


Fig. 2

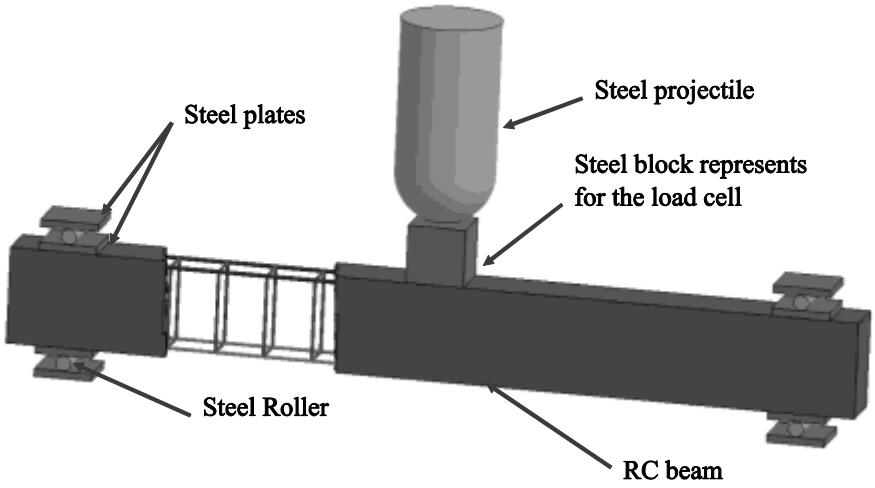


Fig. 3

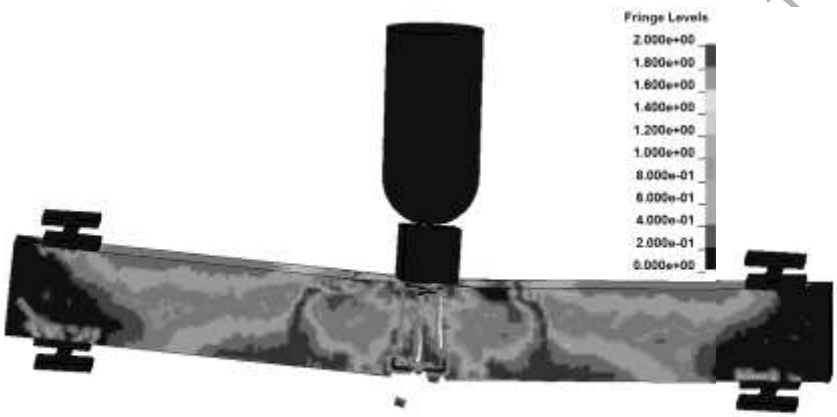


(a) Plastic strain of the RC beam after 0.1 s

(b) Failure of the RC beam after testing

Fig 4

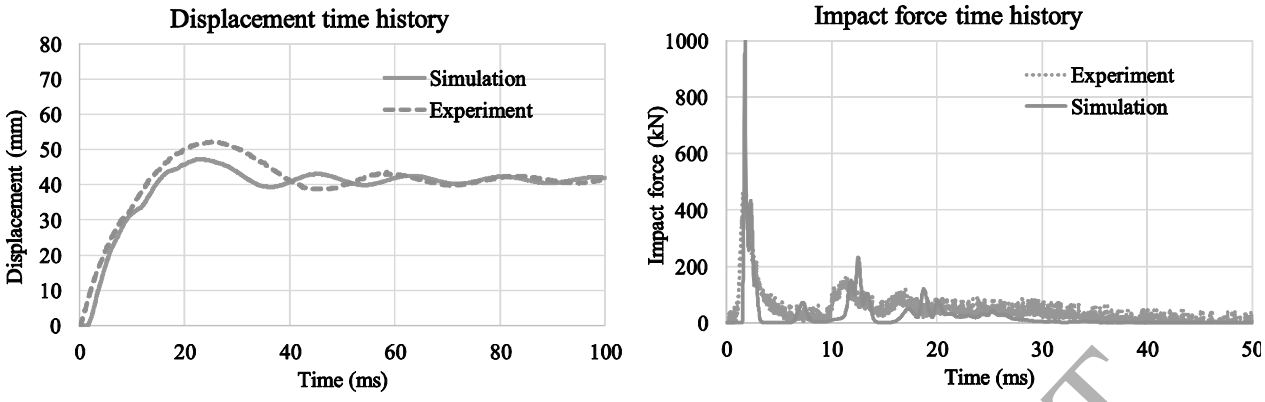


Fig.5

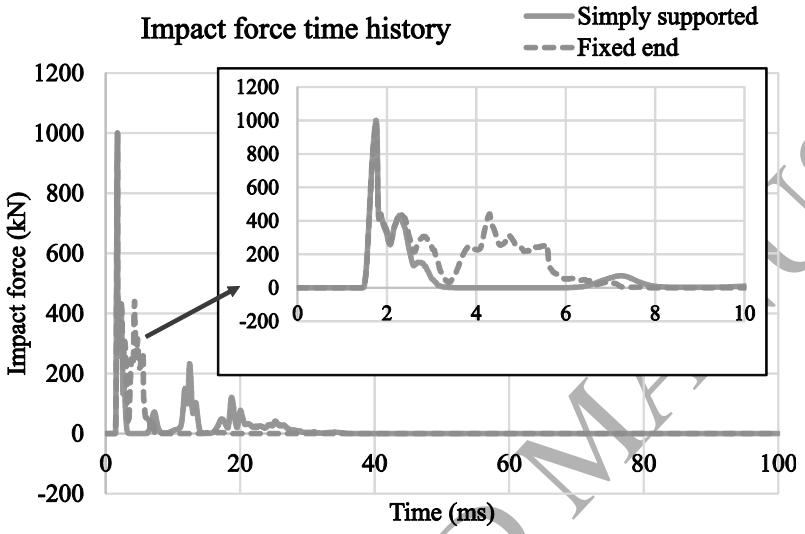


Fig. 6

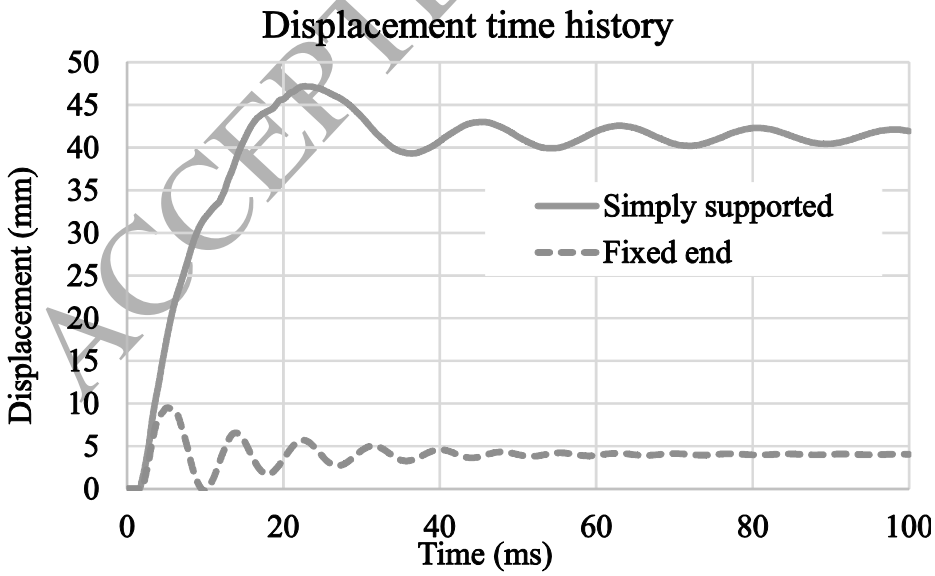


Fig.7

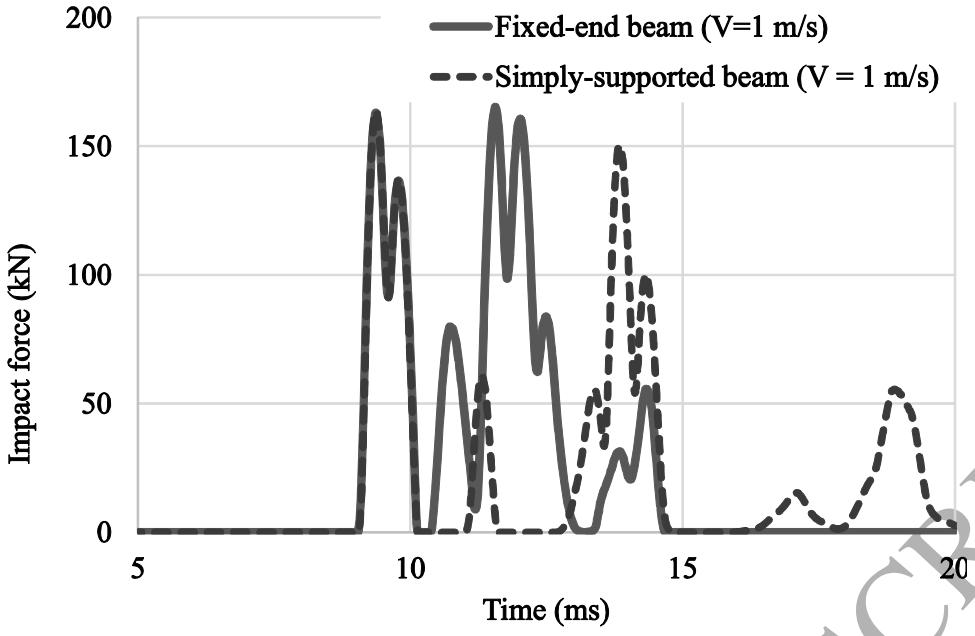


Fig. 8

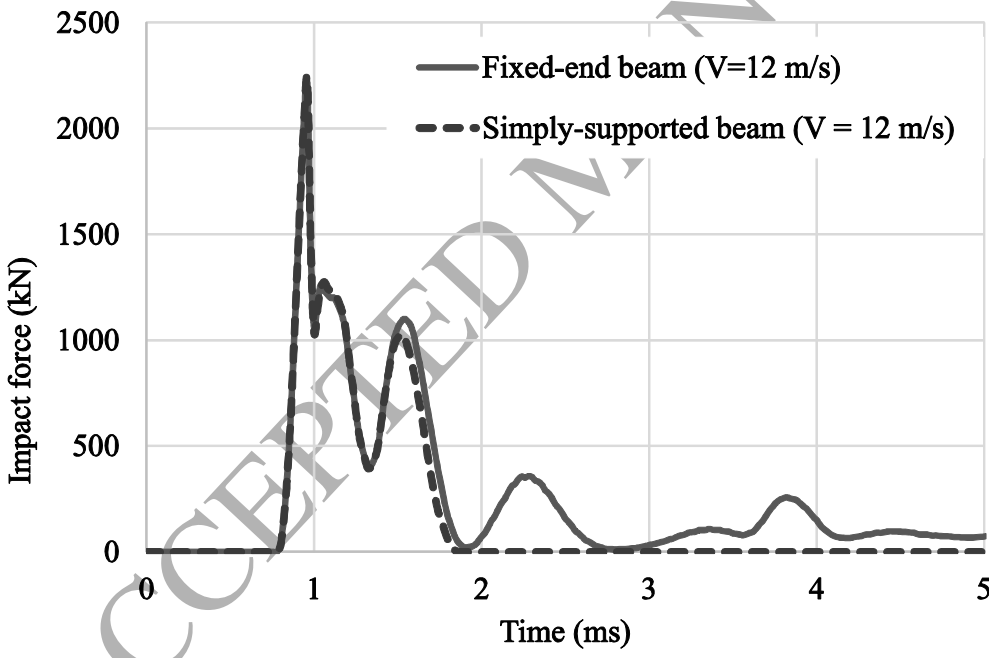


Fig.9

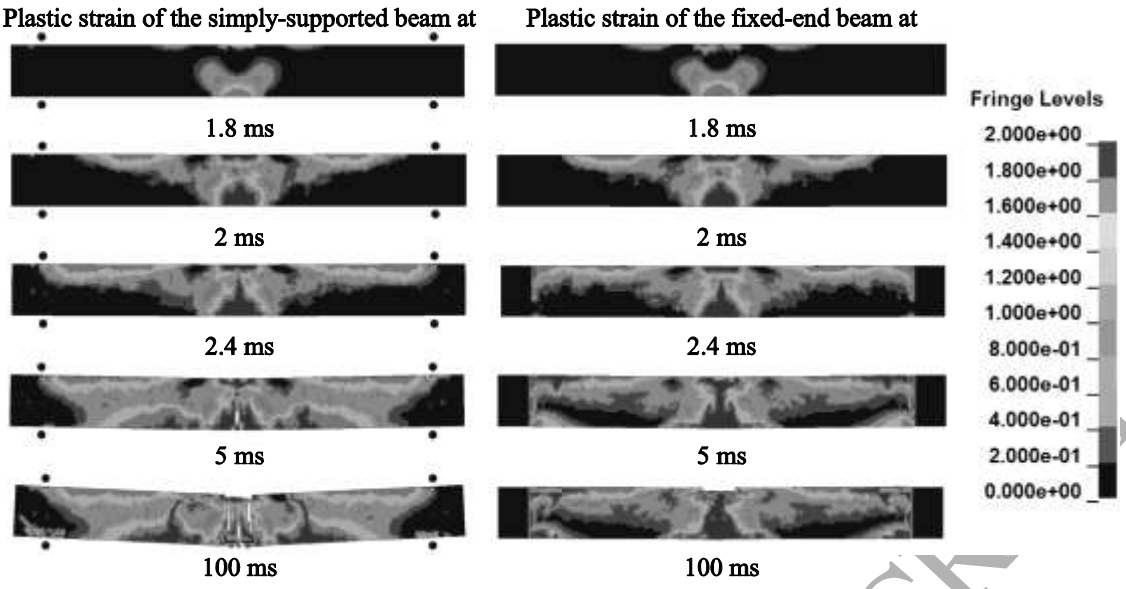


Fig. 10

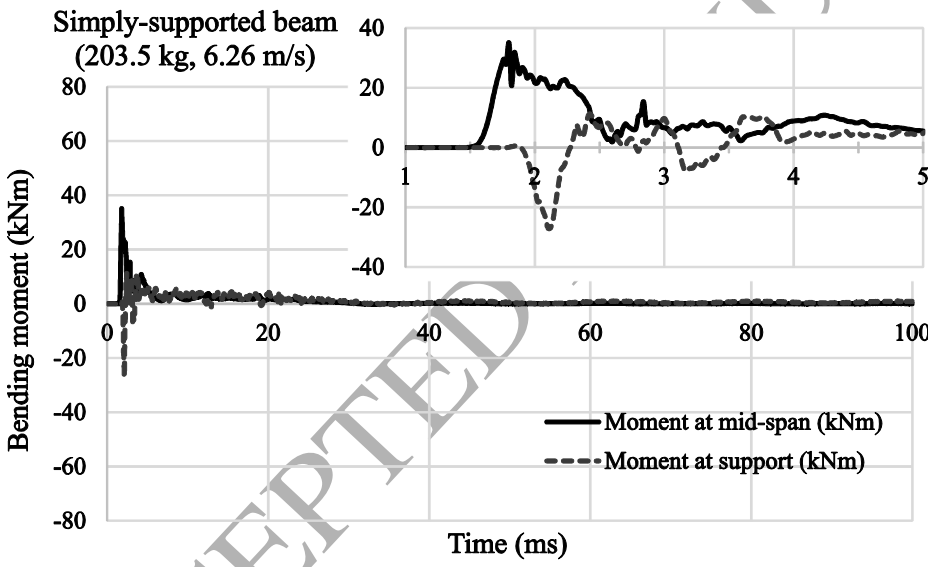


Fig. 11

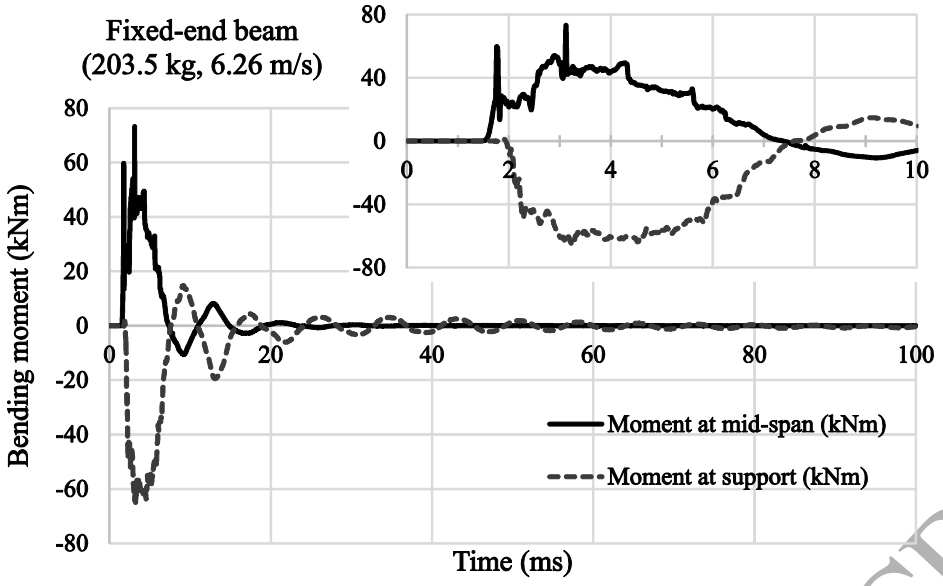


Fig. 12

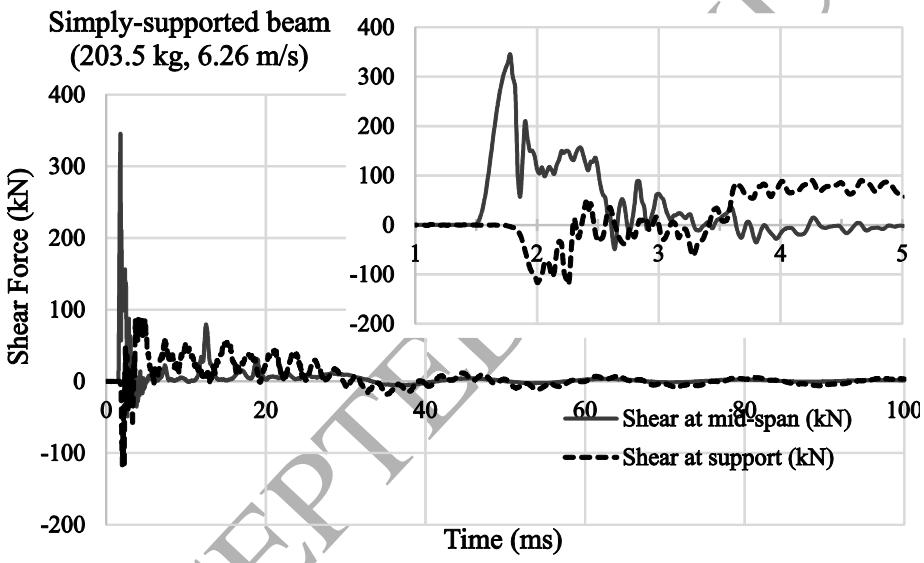


Fig.13

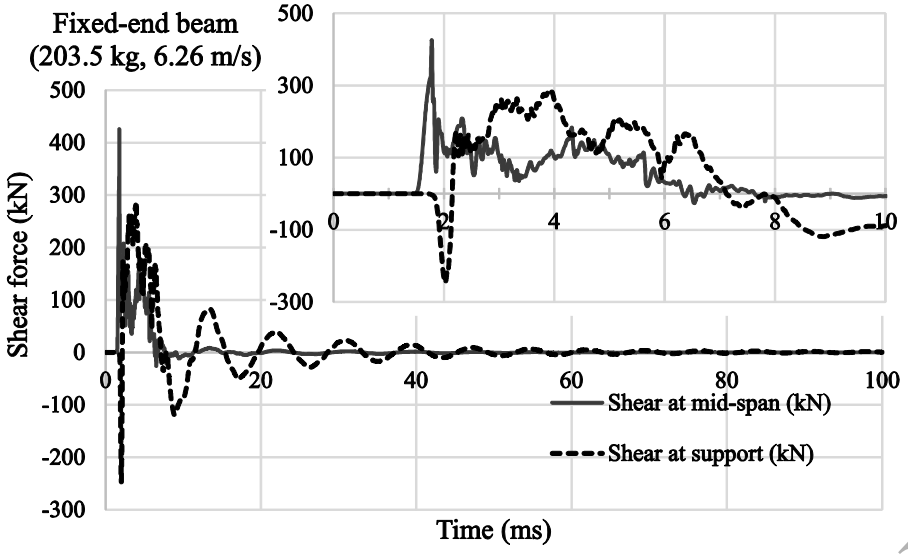


Fig. 14

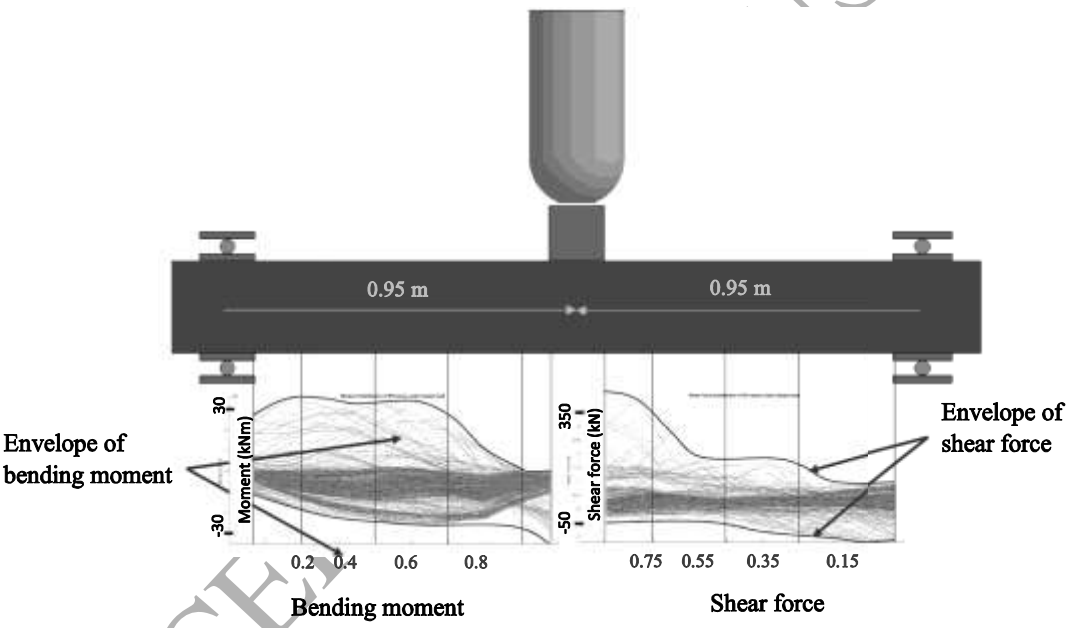


Fig. 15

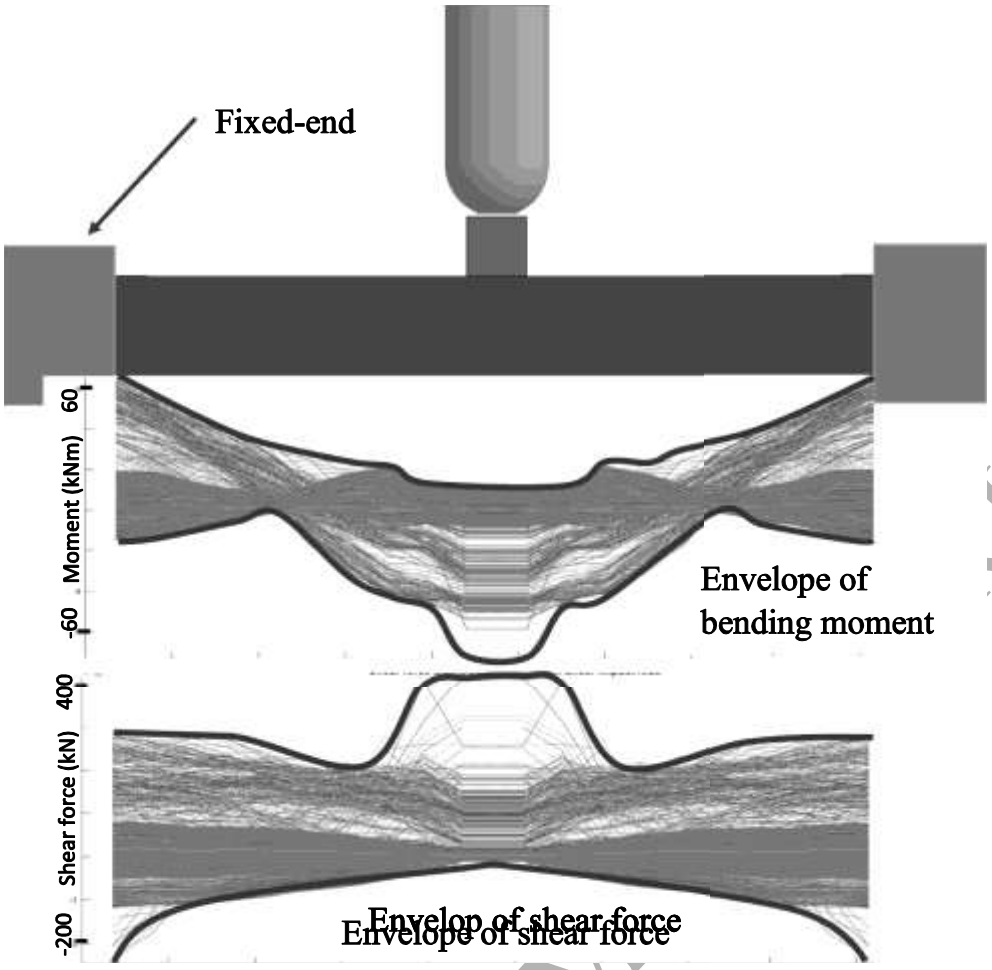
Fixed-end
60
Moment (kNm)
-60
Envelope of
bending moment
400
Shear force (kN)
-200
Envelop of shear force
Envelope of shear force

Fig. 16

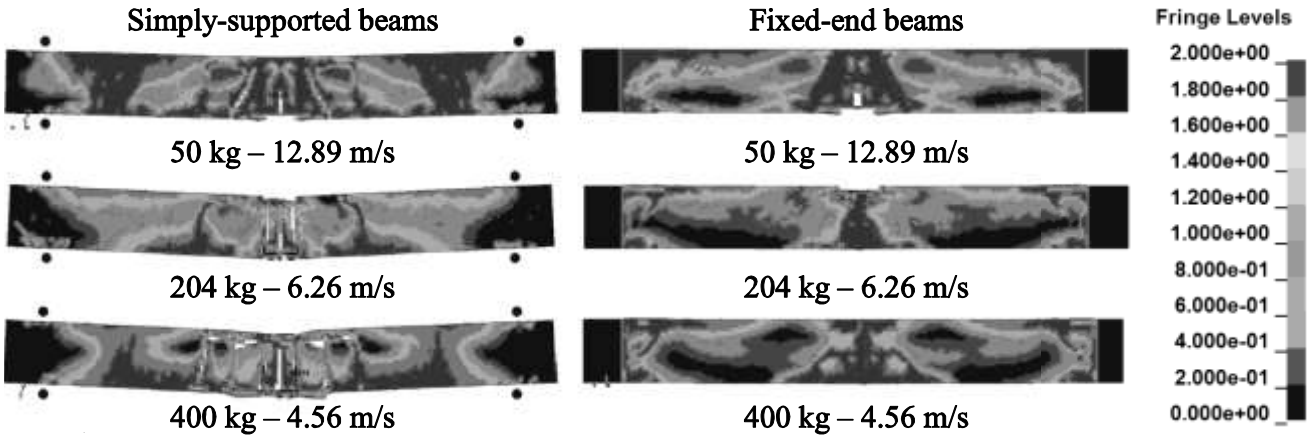
Simply-supported beams
Fixed-end beams
Fringe Levels
2.000e+00
1.800e+00
1.600e+00
1.400e+00
1.200e+00
1.000e+00
8.000e-01
6.000e-01
4.000e-01
2.000e-01
0.000e+00
50 kg – 12.89 m/s
50 kg – 12.89 m/s
204 kg – 6.26 m/s
204 kg – 6.26 m/s
400 kg – 4.56 m/s
400 kg – 4.56 m/s

Fig. 17

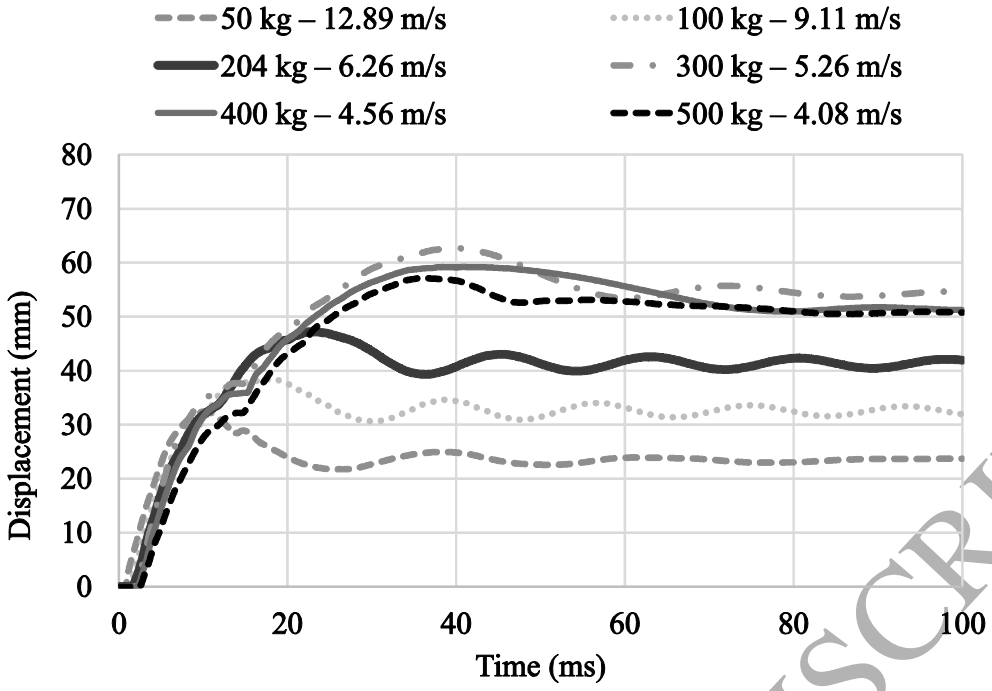


Fig. 18

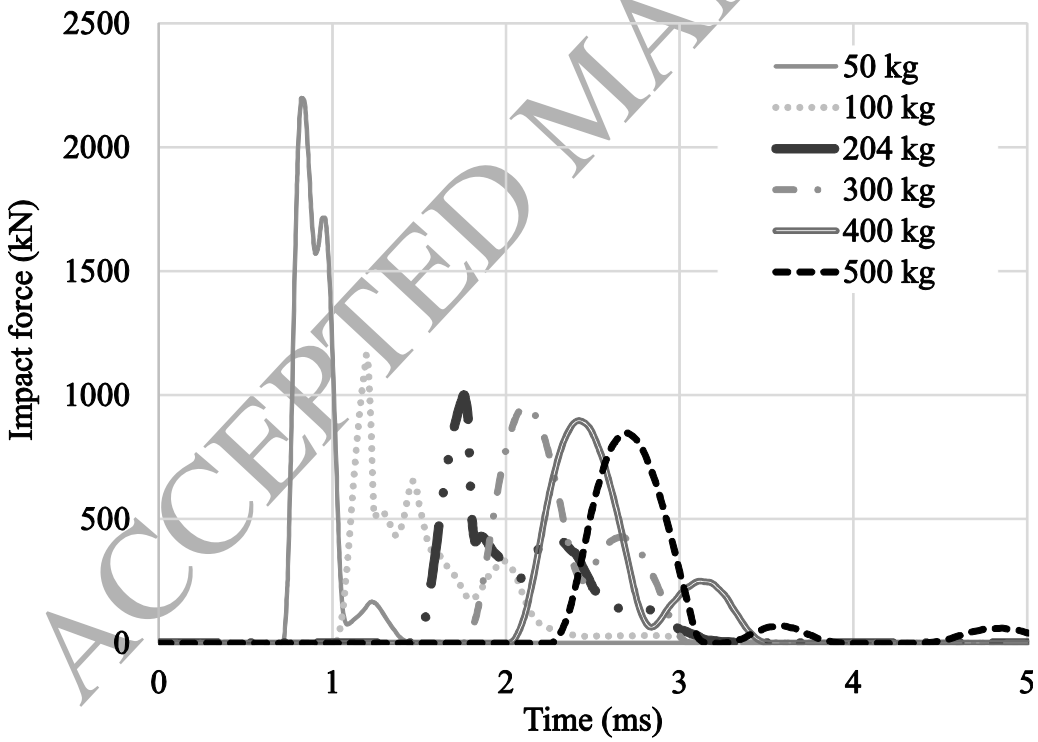


Fig. 19

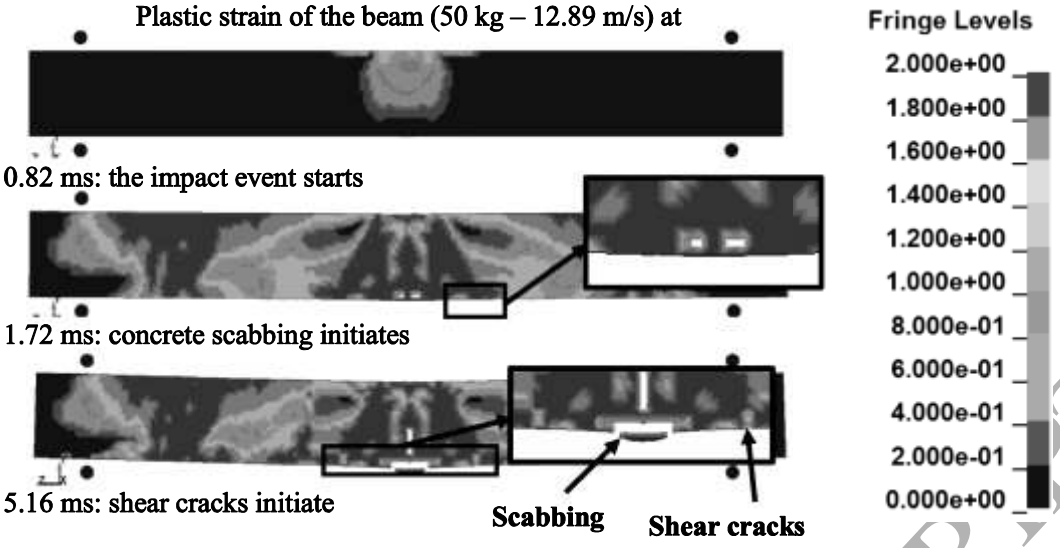
Plastic strain of the beam (50 kg – 12.89 m/s) at
0.82 ms: the impact event starts
1.72 ms: concrete scabbing initiates
5.16 ms: shear cracks initiate
Scabbing
Shear cracks
Fringe Levels
2.000e+00
1.800e+00
1.600e+00
1.400e+00
1.200e+00
1.000e+00
8.000e-01
6.000e-01
4.000e-01
2.000e-01
0.000e+00

Fig. 20

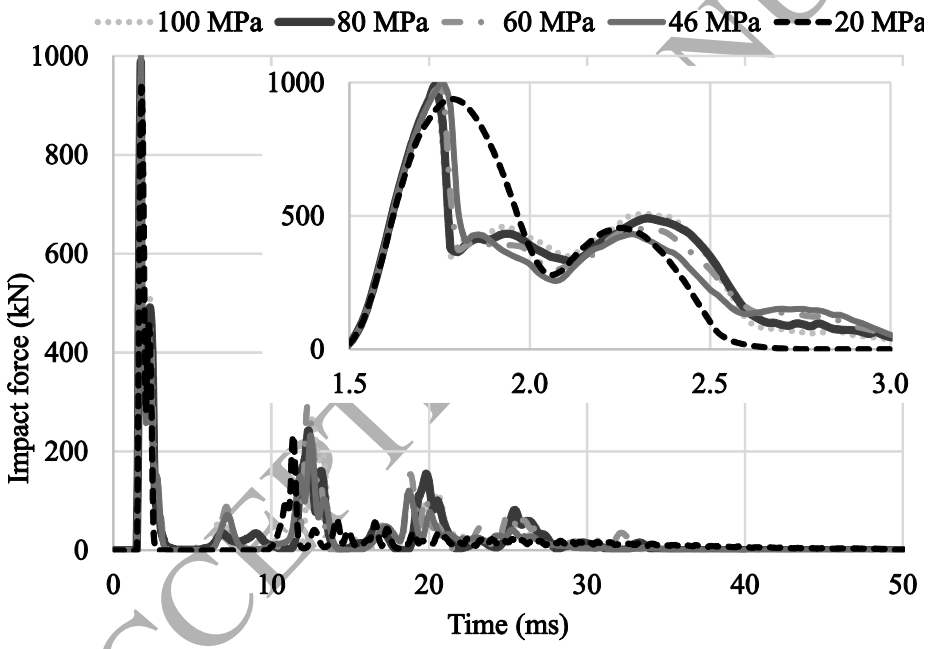
100 MPa
80 MPa
60 MPa
46 MPa
20 MPa
Impact force (kN)
Time (ms)
0
200
400
600
800
1000
0
10
20
30
40
50
0
500
1000
1.5
2.0
2.5
3.0

Fig. 21

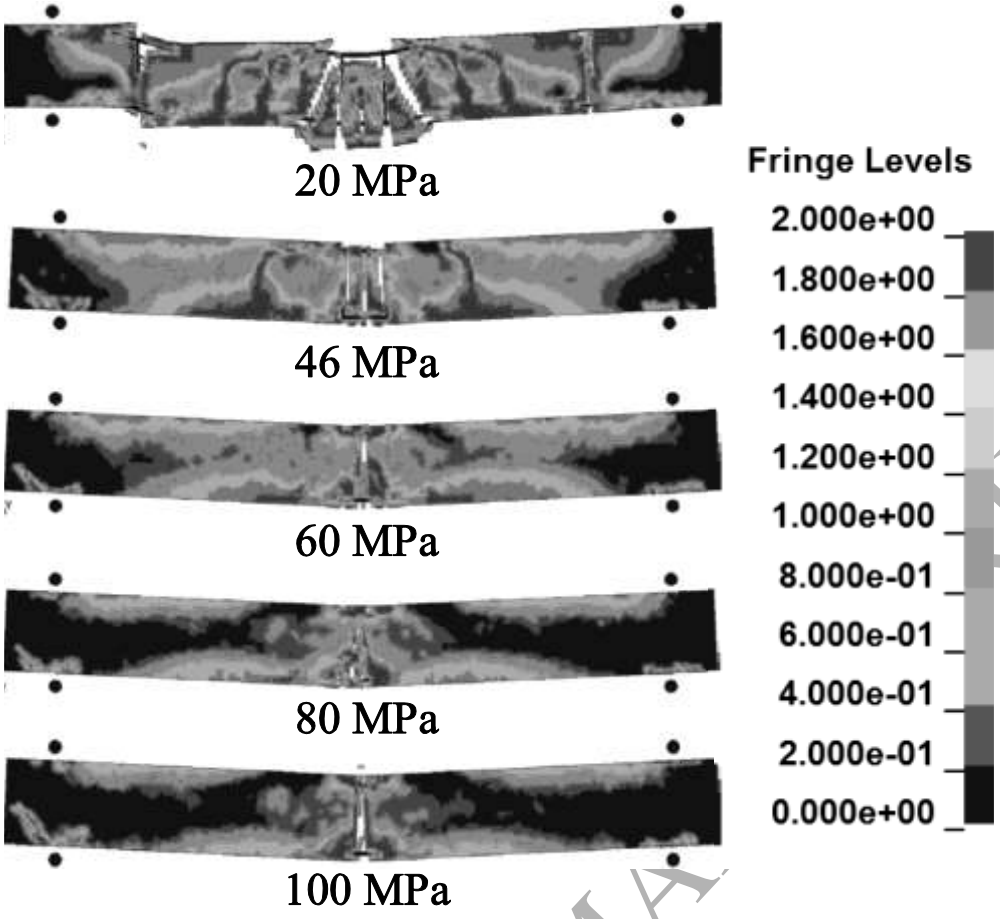


Fig. 22

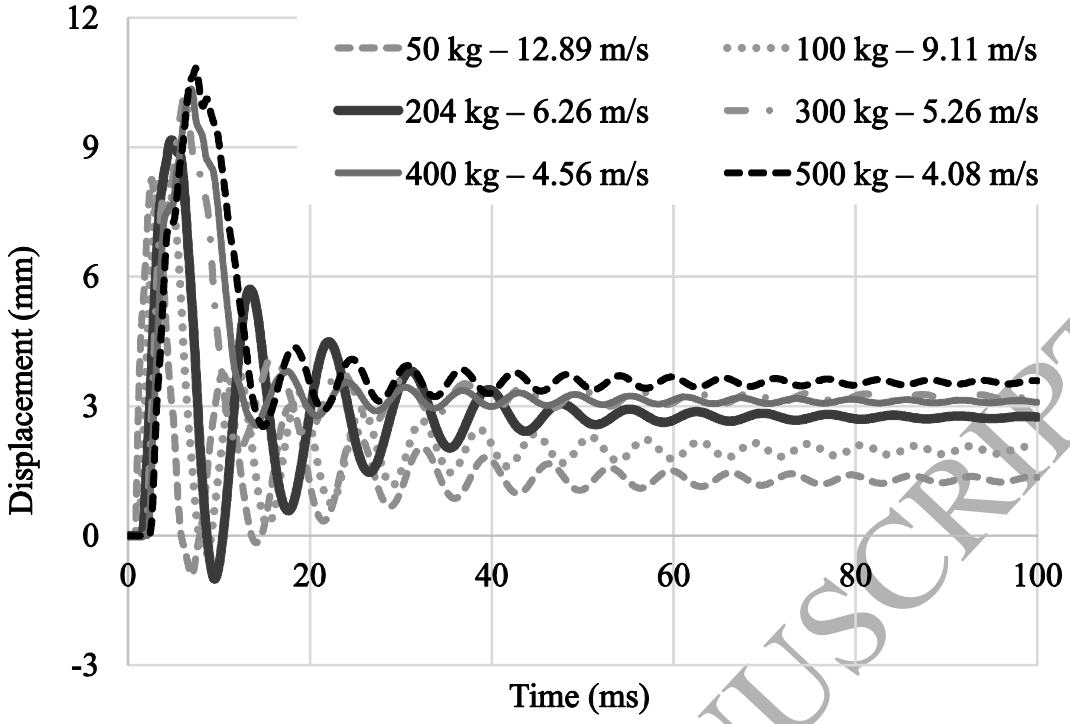


Fig. 23